Structural Engineering and Mechanics, Vol. 42, No. 6 (2012) 831-847
DOI: http://dx.doi.org/10.12989/sem.2012.42.6.831

A one-dimensional model for impact forces resulting from high mass, low velocity debris

K. Paczkowski*[1], H.R. Riggs[1], C.J. Naito[2] and A. Lehmann[2]

[1]Department of Civil and Environmental Engineering, University of Hawaii at Manoa, 2540 Dole Street, Holmes 383, Honolulu, Hawaii 96822, USA
[2]Department of Civil Engineering, Lehigh University, ATLSS Center, 117 ATLSS Drive, IMBT Labs, Bethlehem, PA 18015, USA

(Received December 23, 2011, Revised April 23, 2012, Accepted May 1, 2012)

Abstract. Impact from water-borne debris during tsunami and flood events pose a potential threat to structures. Debris impact forces specified by current codes and standards are based on rigid body dynamics, leading to forces that are dependent on total debris mass. However, shipping containers and other debris are unlikely to be rigid compared to the walls, columns and other structures that they impact. The application of a simple one-dimensional model to obtain impact force magnitude and duration, based on acoustic wave propagation in a flexible projectile, is explored. The focus herein is on in-air impact. Based on small-scale experiments, the applicability of the model to predict actual impact forces is investigated. The tests show that the force and duration are reasonably well represented by the simple model, but they also show how actual impact differs from the ideal model. A more detailed three-dimensional finite element model is also developed to understand more clearly the physical phenomena involved in the experimental tests. The tests and the FE results reveal important characteristics of actual impact, knowledge of which can be used to guide larger scale experiments and detailed modeling. The one-dimensional model is extended to consider water-driven debris as well. When fluid is used to propel the 1-D model, an estimate of the 'added mass' effect is possible. In this extended model the debris impact force depends on the wave propagation in the two media, and the conditions under which the fluid increases the impact force are discussed.

Keywords: debris; tsunami; shipping container; impact force

1. Introduction

A significant threat to structures in the tsunami inundation zone is impact from debris driven by the tsunami flow (NRC 2004); a proper characterization of these forces is especially important to life-safety related to vertical tsunami evacuation shelters (FEMA P646 2008). Debris impact is also an important design consideration for fuel and chemical storage tanks, and port and industrial facilities, all of which may unavoidably be located in tsunami inundation zones. In addition, hurricane or flood-driven, water-borne debris pose similar threats. At port locations, there are often hundreds to thousands of containers. A standard 12.2 m (40 ft) container has an empty weight of

*Corresponding author, Ph.D., E-mail: krystian@hawaii.edu

3,630 kg and a full weight of 30,500 kg; a full container would have a nominal draft of about 0.914 m. A reasonable, expected flow speed could be between 4.5 and 9.0 m/s. Hence, floating containers can pose a significant impact threat to structures in the path of the flow. To properly design structures to resist these demands it is necessary to be able to quantify the impact forces generated by these events.

Debris impact has not received nearly as much attention in the tsunami research community as has the fluid impact forces. Early work considered woody debris, e.g., telephone poles, but recent tsunamis have illustrated that shipping containers are ubiquitous and represent a significant debris threat. Low velocity impact of high mass, water-driven debris on civil-type structures has received attention primarily related to flood-borne woody debris (Haehnel and Daly 2002, 2004, Matsutomi 2009), barge collision on bridge piers (Consolazio *et al.* 2006, Consolazio *et al.* 2009, Consolazio and Cowan 2005), and navigation locks (Arroyo-Caraballo and Ebeling 2006). Impact of shipping containers on waterfront structures has received more attention in Japan (Mizutani *et al.* 2005, Oda *et al.* 2006, Kumagai *et al.* 2006, Yeom *et al.* 2009). A short summary of Japanese studies by Matsutomi and Ikeno are included in FEMA P646 (2008). FEMA P646 also states that more comprehensive studies are required to quantify impact forces.

Code provisions for debris impact forces are based on basic rigid-body impact models and limited experimental data, but despite its importance there is no consensus how to define design impact forces. Debris impact is covered in several codes and design standards. ASCE 7 (2006), the Coastal Construction Manual (CCM) (2005), and FEMA P646 (2008) focus on building structures, while AASHTO (2009) focuses on vessel collision with bridge piers and a US Army Corps of Engineers (USACE) document (2004) focuses on barge impact on navigation locks. Three typical approaches are used to obtain expressions for impact force: impulse-momentum, work-energy, and contact stiffness (Haehnel and Daly 2004, Consolazio *et al.* 2009). Approaches that are based on a physics-based model assume rigid body impact, while the others develop empirical equations to fit experimental data. ASCE 7 takes an impulse-momentum approach involving two rigid bodies, which (ignoring importance and other coefficients) results in

$$F = \frac{\pi m_p v_f}{2\Delta t} \tag{1}$$

in which F is the impact force, m_p is the total mass of the projectile (i.e., the debris), v_f is the impact velocity, and Δt is the time to reduce the debris velocity to zero. An impact duration of 0.03 s is recommended. CCM takes a similar approach, but has recommended values for Δt ranging from 0.1 to 1.0 s, resulting in an order of magnitude difference in impact force (Robertson *et al.* 2006). Clearly, there is no clear choice for the impact duration (FEMA P646 2008).

FEMA P646 (2008) follows the formulation proposed by Haehnel and Daly (2002, 2004), which is based on the impact of two rigid bodies with a contact stiffness between them. Their equation for impact force is

$$F = v_f\sqrt{k_c m_p} \tag{2}$$

in which k_c is a contact stiffness that must be determined experimentally. FEMA P646 modified this equation by adding a force amplification factor of 2.0 to include the 'added mass' effect, i.e., the increase in force from the presence of the water. There was no justification for the value selected. Some other manuals also include a force increase for the water inertia (AASHTO 2009), although much less than double.

Work-energy for debris flow is not used in this country, although it can be shown that all three approaches are identical if certain assumptions are made (Haehnel and Daly 2004). AASHTO (2009) considers work-energy for vessel collisions with bridge piers, but the force equations are based more on empirical data than on a physical model. The commentary points towards recent work (Consolazio *et al.* 2006), indicating that a more refined, analysis-based procedure is needed. Excluding the empirical, data-driven AASHTO and USACE equations, the presented approaches are all based on impact of rigid bodies. However, a shipping container impacting a concrete column or wall, or even a steel column, is not rigid compared to the structure it strikes. In fact, for a prototypical 68.6 cm square concrete column (Mikhaylov 2009) being hit by a shipping container, the column is essentially rigid compared to the container (based on static stiffness). Furthermore, the application of rigid body impact theory is appropriate if the duration of impact is much larger than the natural period of the bodies (Goldsmith 1960); this is not the case with the debris.

The impact model proposed herein involves a flexible, elastic projectile hitting a rigid wall (a flexible wall can be included by extension of the theory). The impact forces are determined based on the acoustic-wave propagation in the projectile. The fluid behind the projectile is included, in an effort to quantify the ‘added mass’ effect. In Section 2, the analytical model is presented. Section 3 discusses the experimental setup used to obtain data to validate the impact model. Results are discussed in section 4, including validation of the numerical model, while the finite element model is presented in section 5. Section 6 contains conclusions from the present study and suggestions for future work.

2. One-dimensional analytical model

The water-borne projectile is modeled as an elastic bar of length L_p pushed along by a semi-infinite horizontal column of fluid, as depicted in Fig. 1. The projectile is propelled to the left with speed v_f. When the left end of the projectile hits the ‘wall’, an acoustic wave propagates from left to right. The one-dimensional wave equation governs the acoustic wave in both the projectile and the fluid

$$\frac{\partial^2 u(x,t)}{\partial t^2} - c^2 \frac{\partial^2 u(x,t)}{\partial x^2} = 0 \tag{3}$$

in which $u(x, t)$ is the displacement field and c is the speed of sound in the medium. In the projectile, the speed of sound is given by

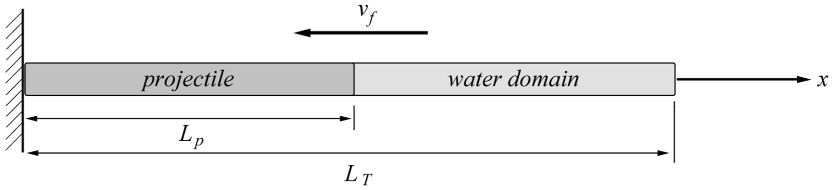

Fig. 1 Projectile and water column

$$c_p = \sqrt{\frac{E_p}{\rho_p}} \tag{4}$$

in which E_p is the Young's modulus and ρ_p is the mass density. The water is characterized by the speed of sound c_f, mass density ρ_f, and the bulk modulus $K_f = c_f^2 \rho_f$.

2.1 Impact without water

First consider the case of the projectile hitting a rigid wall with no fluid. In that case the initial conditions are

$$u(x, 0) = 0, \quad \dot{u}(x, 0) = -v_f \tag{5}$$

and the boundary conditions are

$$u(0, t) = 0, \quad u_{,x}(L_p, t) = 0 \tag{6}$$

To impose the zero displacement at the left end, one can write for a differential segment the constraint at impact

$$-v_f dt - \varepsilon_p dx = 0 \tag{7}$$

in which ε_p is the strain in the projectile. Eq. (7) results in

$$\varepsilon_p = -\frac{v_f}{dx/dt} = -\frac{v_f}{c_p} \tag{8}$$

The force in the projectile at $x = 0$ (i.e., the impact force on the wall) is then given by

$$F = -\frac{E_p A_p}{c_p} v_f = -c_p \rho_p A_p v_f = -\sqrt{E_p \rho_p} A_p v_f = -\sqrt{k_p m_p} v_f \tag{9}$$

in which A_p is the structural area of the projectile, $k_p = E_p A_p / L_p$, and $m_p = \rho_p A_p L_p$. Eq. (9) is a well-known result. Note that this force does not depend on the total projectile mass, as is assumed in Eqs. (1) and (2). The impact force is constant as the stress wave propagates down the projectile until it reaches the free end at time $t_L = L_p/c_p$. It is then reflected back to maintain the stress free condition at $x = L_p$. Hence, the force in the projectile is

$$F = \begin{cases} -\dfrac{E_p A_p}{c_p} v_f H(c_p t - x), & 0 \le t \le t_L \\ -\dfrac{E_p A_p}{c_p} v_f H[2c_p(t_L - t) - x], & t_L \le t \le 2t_L \end{cases} \tag{10}$$

in which H is the Heaviside step function. At time $2t_L$ the reflected wave has reached the wall. The force would then become tensile, except this means the projectile separates from the wall and the impact is over. Hence, the constant force of impact is given by Eq. (9) and its duration, t_D, is $2t_L$.

2.2 Non-dimensional formulation

At this point it is worthwhile to nondimensionalize the formulation. Length variables are nondimensionalized by L_p, such that $\bar{x} = x/L_p$ and $\bar{u} = u/L_p$. Nondimensional time is $\bar{t} = t/t_L = tc_p/t_L$,

while nondimensional force $\bar{F} = F/\left(-\frac{E_pA_p}{c_p}v_f\right)$. The result is to nondimensionalize velocity by c_p. The wave equation becomes

$$\frac{\partial^2\bar{u}}{\partial\bar{t}^2} - \frac{\partial^2\bar{u}}{\partial\bar{x}^2} = 0 \tag{11}$$

with initial conditions

$$\bar{u}(\bar{x}, 0) = 0, \quad \dot{\bar{u}}(\bar{x}, 0) = -\bar{v}_f \tag{12}$$

and boundary conditions

$$\bar{u}(0, \bar{t}) = 0, \quad \bar{u}_{,\bar{x}}(1, \bar{t}) = 0 \tag{13}$$

2.3 Contact stiffness without water

Now consider the case where there is a Hertzian-type contact stiffness between the projectile and the wall (alternatively, the wall can be viewed as flexible but massless). The stiffness is represented by a simple linear spring of stiffness k_c. The nondimensional stiffness is defined as $\bar{k} = k_c/(E_pA_p/L_p)$. The initial conditions are unchanged, but the boundary condition at the left is

$$\bar{k}\bar{u}(0, \bar{t}) - \bar{u}_{,\bar{x}}(0, \bar{t}) = 0 \tag{14}$$

which simply states that the force in the contact spring is equal to the force in the projectile at the contact point.

The solution can be represented fairly simply using the well-known separation of variables and modal superposition method. That is, the solution is of the form

$$\bar{u}(\bar{x}, \bar{t}) = \sum_{n=0}^{\infty}\phi_n(\bar{x})Y_n(\bar{t}) \tag{15}$$

For the given initial and boundary conditions, the solution is

$$\bar{u}(\bar{x}, \bar{t}) = -\bar{v}_f\sum_{n=0}^{\infty}\frac{\dot{Y}_n(0)}{z_n}\sin(Z_n\bar{t})\phi_n(\bar{x}) \tag{16}$$

in which

$$\dot{Y}_n(0) = \frac{4}{2Z_n\left(\frac{z_n^2}{\bar{k}^2} + \frac{1}{\bar{k}} + 1\right) - \frac{2Z_n}{\bar{k}}\cos(2Z_n) + \left(\frac{z_n^2}{\bar{k}^2} - 1\right)\sin(2Z_n)} \tag{17}$$

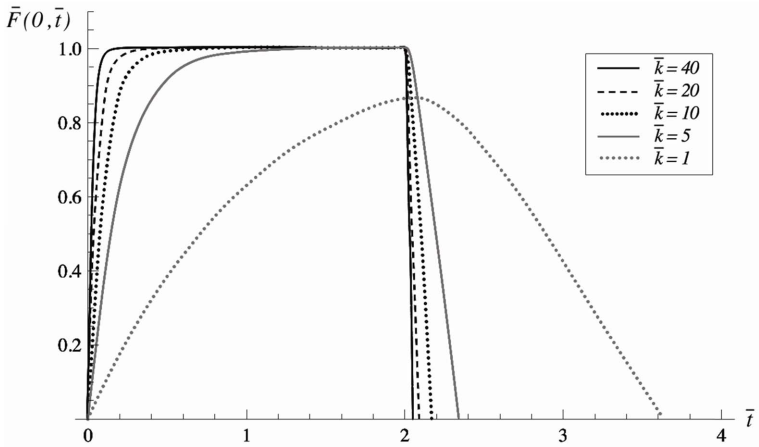

Fig. 2 Nondimensionalized force vs. time for different values of stiffness ratio $\bar{k}$

and

$$\phi_n(\bar{x}) = \sin(Z_n\bar{x}) + \frac{Z_n}{\bar{k}}\cos(Z_n\bar{x}) \tag{18}$$

Z_n are the eigenvalues determined from

$$Z_n\tan(Z_n) = \bar{k} \tag{19}$$

The nondimensional force on the wall can then be determined as

$$\bar{F}(0,\bar{t}) = \sum_{n=0}^{\infty}\dot{Y}_n(0)\sin(Z_n\bar{t}) \tag{20}$$

A convergence study showed that the larger the number of terms in the Fourier series, the less oscillation around the maximum expected non-dimensional value of 1.0, and that higher $\bar{k}$ values required a larger number of terms. For the values of $\bar{k}$ that were tested, 50 terms in the series was sufficient to obtain the force within 0.001 of the expected maximum non-dimensional force. The results for different $\bar{k}$ values are presented in Fig. 2. For a rigid contact stiffness, $\bar{F} = 1$ and the nondimensional duration is 2. The results show that for $\bar{k} = 40$, the response is nearly the same as for rigid contact. As $\bar{k}$ decreases, the duration increases and the maximum impact force eventually begins to decrease, compared to the impact force with rigid contact.

2.4 Fluid-driven impact

To estimate the influence of the water on the impact force, the water is modeled as an infinitely long column of water behind the projectile (Fig. 1), or at least sufficiently long such that during the time of interest acoustic waves in the water propagate only in the $+x$ direction. The water is confined to the column, and hence there is only one-dimensional wave propagation. This is a conservative assumption, as it will overestimate the influence of the fluid on the impact force. The water and projectile are assumed to have the same initial velocity, $-v_f$. The fluid pressure is defined by $\rho = K\varepsilon_v$, where ε_v is the volumetric strain. However, in this case $\varepsilon_v = \partial u/\partial x$ in the fluid.

At the interface between the projectile and the fluid, the velocities of the projectile and fluid must be equal, which in this case means the displacements are equal. Similarly, the force in the projectile at $\bar{x} = 1$ must be equal to the integrated pressure in the fluid. Some projectiles, such as a shipping container, will have an area A_f exposed to the fluid that is much different than the structural area A_p that contributes to the stiffness E_pA_p. The nondimensional interface area is defined as $\bar{A} = A_f/A_p$. The compatibility equation for force can then be written as

$$\bar{u}_{p,\bar{x}} = \bar{c}^2\bar{\rho}\bar{A}\bar{u}_{f,\bar{x}} \tag{21}$$

in which $\bar{c} = c_f/c_p$ and $\bar{\rho} = \rho_f/\rho_p$.

The fluid will not feel the impact until the stress wave reaches the interface at time $\bar{t} = 1$. At that time, part of the wave will be transmitted to the fluid and part will be reflected back from the interface. The interface can be replaced by reflection and transmissibility coefficients, R and T, respectively, that give the proportions of the wave that are reflected by the fluid interface and transmitted to the fluid. Expressions for the coefficients are obtained by imposing the interface conditions, and are

$$R = \frac{\bar{A}\bar{c}\bar{\rho} - 1}{\bar{A}\bar{c}\bar{\rho} + 1} \tag{22}$$

and $T = 1 + R$. Note that $-1 \le R \le 1$. When the fluid is air, then $R = -1$ and all the wave is reflected back; this is the case discussed in section 2.1. When the projectile and the fluid are the same material and $\bar{A} = 1$, $R = 0$ and there is no reflection. In this case the impact force is $\bar{F} = 1$ and it lasts for infinity. In general, however, the wall will feel the reflected wave at $\bar{t} = 2$. The force it feels at that time is $(1 + R)$. The reflected wave is again reflected at the wall. For a rigid wall, the reflection is 100% and the force after reflection is $(1 + 2R)$. If $R < 0$, the fluid does not increase the magnitude of the impact force, and if $R > 0$, the fluid will increase the impact force. Hence, it appears that it may be possible to use R to quantify the effect of the so-called 'added mass', in the sense of how much the fluid increases the impact force.

By considering the waves propagating back and forth, the following series for the force at the wall can be obtained

$$\bar{F} = 1 + 2R + 2R^2 + 2R^3 + 2R^4 + 2R^5 + 2R^6 + 2R^7 + 2R^8 + \ldots \tag{23}$$

The first term is the initial impact force, $1 + 2R$ is the force starting at $\bar{t} = 2$, $1 + 2R + 2R^2$ is the force starting at $\bar{t} = 4$, etc. Clearly, the sequence should stop when $\bar{F} \le 0$, at which point separation occurs. If $R \le 0.5$, separation occurs at $\bar{t} = 2$. If $R > -0.5$, separation never occurs and hence the duration of impact increases. The asymptotic value of Eq. (23) is $\bar{A}\bar{c}\bar{\rho}$. Especially when the fluid increases the force, it is unlikely the above formula is applicable beyond a cycle or two, after which three-dimensionality effects in the water will likely predominate. Any amplification in the force as a result of the fluid is likely limited to $(1 + 2R)$ or less.

Typical debris will be either steel (e.g., shipping containers) or wood (logs and telephone poles). If it is assumed that for seawater $\rho_f = 1025$ kg/m^3 and $c_f = 1560$ m/s, and for steel $\rho_p = 7850$ kg/m^3 and $c_p = 5960$ m/s, then $\bar{\rho} = 0.13$ and $\bar{c} = 0.26$. For wood with $\rho_p = 550$ kg/m^3 and $c_p = 3500$ m/s, $\bar{\rho} = 0.54$ and $\bar{c} = 0.45$. For the water to increase the duration of impact, $R > -0.5$. From Eq. (22), this implies $\bar{A}\bar{c}\bar{\rho}$ > 1/3. This corresponds to $\bar{A}$ > 9.8 for a fully submerged steel projectile and $\bar{A}$ > 1.4 for a fully submerged wood projectile. If a log or telephone pole is half-submerged, the nondimensional area would be around 0.5, and therefore for woody debris it is likely that the fluid will not increase the impact duration or force (even if it were fully submerged). However, for typical shipping container dimensions, the container end area is approximately 800 times the structural area, i.e., the area of the longitudinal beams at the four corners. Although it depends on the draft, R may be greater than 0.8 This model, which provides a conservative (upper bound) estimate of the fluid effect, predicts that the maximum impact force might be nearly 2.5 to 3 times (based on $1 + 2R$) to what it would be in-air. In addition, separation will not occur.

3. Experimental setup

Small-scale experiments were conducted to compare the one-dimensional (in-air) impact model with real impact data. The experimental setup was developed to represent direct, head-on impact by a projectile. The projectiles consisted of a standard rectangular steel tube 5.08 cm × 5.08 cm × 0.3175 cm, Fig. 3. The projectile traveled along a guide system fabricated from steel angle sections. The rail guide helped to obtain a direct impact. A 244 kN (55 kip) load cell (model MTS 661.23A-01) attached to a stiffened angle bracket represented the wall, Fig. 3. A protective plate was bolted to the front of the load cell. The railing system was designed such that the impact occurred at the center of the load cell.

Four different length projectiles were used: 1, 2, 3, and 4 m long. Each projectile was instrumented with resistance-based strain gauges at three cross sections along the length: 5 cm from the front, in the middle, and 5 cm from the rear. At each instrumented cross-section, a strain gauge was placed on the front and back sides of the tube. The strain sensors allowed the forces in the

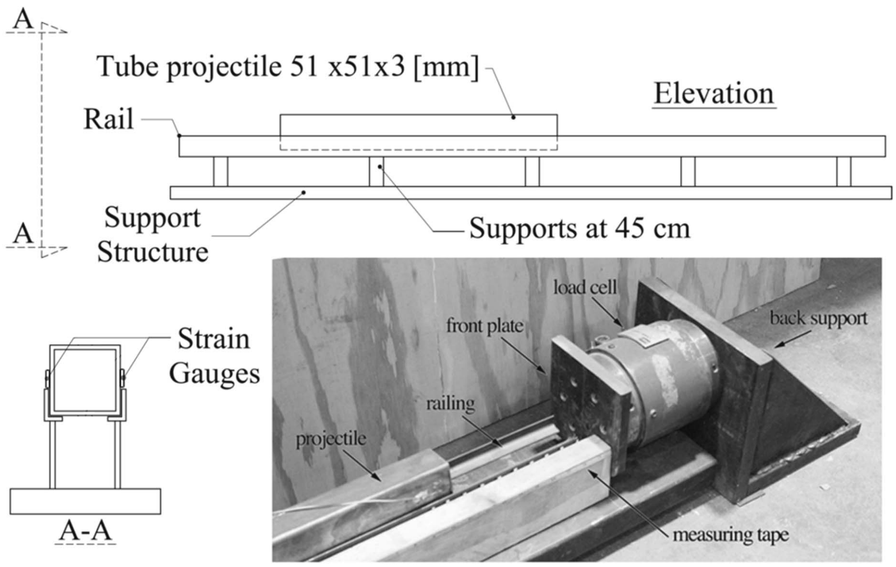

Fig. 3 Experimental impact setup

projectiles to be compared to the forces measured by the load cell, and to observe the wave propagation. Half of the trials for each projectile recorded strains only from the front two strain sensors. This allowed for a marginally higher recording frequency. Depending on the test configuration, data were recorded between 25 kHz and 50 kHz, with most of the data recorded around 30 kHz.

The projectile was accelerated manually down the guide track. Impact velocity was determined through the use of high-speed video (1000 frames per second) and a fixed scale attached to the setup. The time stamp over a 2 cm length (i.e., when the debris was at 3 cm and 1 cm from the impact plate) was used to determine the impact velocity. The location was determined with an accuracy of 0.5 mm and, based on the frame rate, the time stamp was determined with an accuracy of 0.5 msec. The error for the velocity measurements is therefore estimated at approximately ±6%. Eq. (9) implies that the error in force based on the measured velocities will have a similar error.

The mass of the load cell was 14.916 kg, the 15 cm × 15 cm × 2 cm front plate had a mass of 3.376 kg, and the six screws that bolted the plate to the load cell were 0.082 kg total. The total mass of the load cell setup, which was bolted to the back support, was 18.374 kg. The manufacturer-provided stiffness for the load cell is 2.97×10^6 kN/m (17×10^6 lbf/in).

In the following, the projectile properties are taken to be E_p = 210 GPa, A_p = 5.42 cm^2, and ρ_p = 7850 kg/m^3. Based on the load cell stiffness and the area and modulus of the projectile, $\bar{k}$ varied from 26 for the 1 m projectile to 104 for the 4 m projectile. From Fig. 2, it was anticipated that the results would be similar to the rigid wall response in section 2.1.

4. Results

Twelve trials were run for each of the four projectile lengths. Of the 48 trials, not all the data recorded properly in 4 trials, resulting in 44 trials with a full complement of data. During the trials, the force in the load cell and strains in the projectiles were measured. Figs. 4-7 present the load cell force-time history results for four projectile lengths. For clarity in the figures, only some of the recorded trials are presented. All twelve trials for each of the projectiles had very similar time histories. The measured forces have been non-dimensionalized by the theoretical impact force from Eq. (9), i.e., 22.0 v_f kN, where v_f is in m/s. As illustrated, the trials produced repeatable results with similar histories and maxima. This behavior is typical of the other trials conducted. Variations between the cases shown may be related to uneven impact against the front plate due to, e.g., the moderate lateral tolerances in the guide rail, the manual acceleration of the projectile, and/or fabrication tolerance of the tube face.

The theoretical impact force time history due to the projectile impacting a rigid wall is compared to the measured reaction force in Figs. 4-7. As illustrated, the proposed model provides a good approximation of the expected maximum impact force and duration. The gradual increase in impact force, as compared to the sudden jump in the 1-D model, may be caused by uneven contact surfaces between the projectile and the front plate on the load cell, resulting in a finite contact stiffness. It should also be noted that the theory gives the impact force, whereas the experiments measured the force in the load cell. Analysis of the free-vibration response of the load cell after impact revealed that the first natural period of the load cell and support bracket combination was approximately 4 ms for the 1, 2 and 3 m projectiles and 3.6 ms for the 4 m projectile (reassembling the test setup between these two sets of experiments led to the change in period). The oscillations in the measured

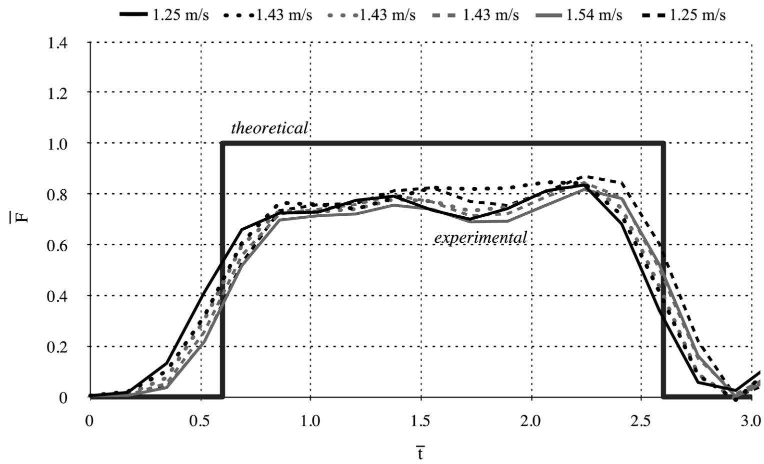

Fig. 4 Normalized load cell histories for 1 m projectile

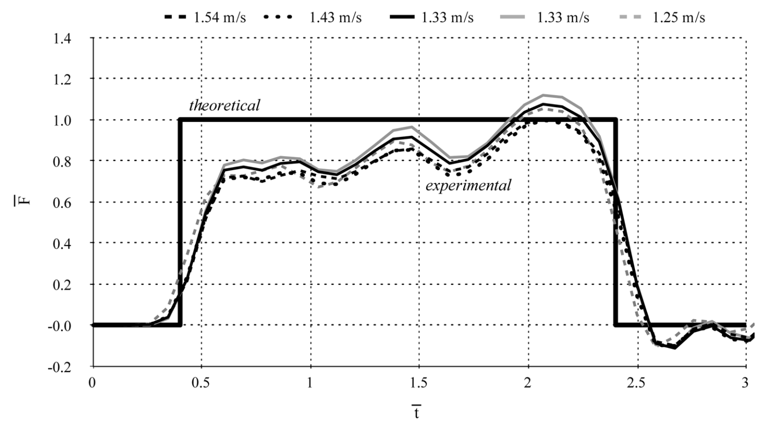

Fig. 5 Normalized load cell histories for 2 m projectile

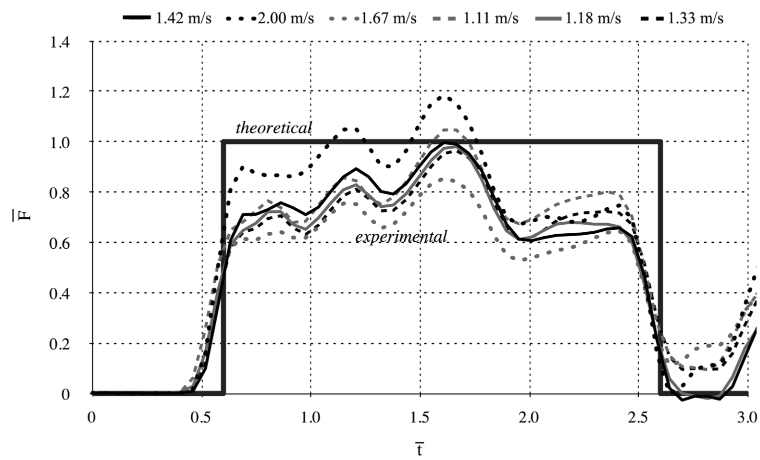

Fig. 6 Normalized load cell histories for 3 m projectile

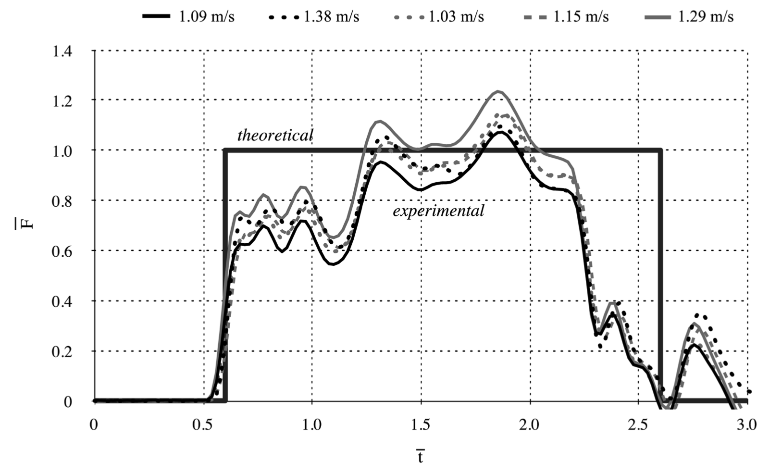

Fig. 7 Normalized load cell histories for 4 m projectile

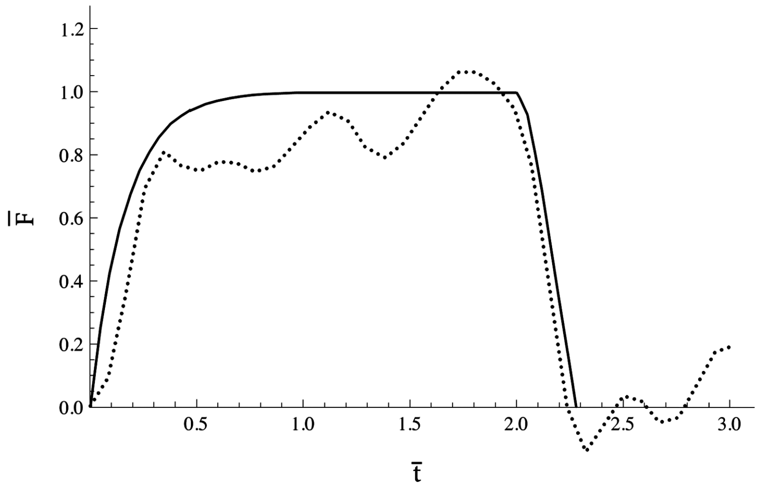

Fig. 8 Response with contact stiffness $\bar{k}$ = 6.0: dotted black line is experimental data for 2 m projectile; solid black line is calculated result

forces during impact that are observable in Figs. 4-7 have a period of approximately 0.20-0.22 ms, well below the first natural period of the load cell assembly.

Results in Figs. 4-7 indicate that the experimental setup is a less controlled configuration than the split Hopkinson bar (Johnson 1972). However, the configuration probably presents a more realistic scenario of debris impact that will be experienced in the field. The increasing oscillation with increasing projectile length indicate that as the duration of impact increases, the structure has more time to respond dynamically. The noticeable force oscillations are not a result of the fundamental frequency of the load cell; rather, it is likely that they are a result of higher frequencies of the load cell. The gradual rather than abrupt increase in impact force is consistent with other impact experiments (Johnson 1972). To represent a more gradual impact demonstrated by the experimental forces, results for the model with a contact stiffness were obtained for the 2 m projectile. To match

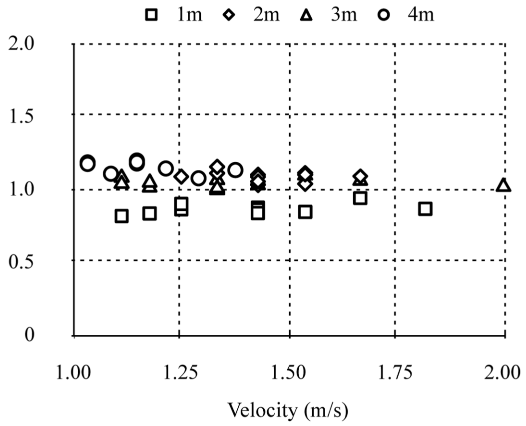

Fig. 9 Normalized measured impact force versus impact velocity

the slope in the force time history, a value of $\bar{k} = 6.0$ was used. Results are compared in Fig. 8. The dotted black line represents one of the experimental trials (2 m long projectile with 1.67 m/s velocity) and the black solid line shows the calculated force. The one-dimensional model seems to provide a reasonable approximation with the measured forces.

The nondimensionalized maximum force in the load cell versus impact velocities for recorded cases is shown in Fig. 9. These results agree with the proposed one-dimensional analytical model ($\bar{F} = 1$). The variation in the measured impact force relative to the theoretical force ranges from 0% to 27%. For the 1 m, 2 m, 3 m, and 4 m projectiles, the average errors were 20%, 5%, 2% and 11%, respectively. The largest discrepancy occurred for the 1 m projectile, the reason for which is unclear; it could be that the smaller mass was insufficient to ensure full contact with the plate after the impact. The magnitude of error for the 4 m projectile is due likely to the specimen length, which was longer than the rail guide. To provide physical scale, it is noted that the impact force from Eq. (9) is 22 kN at 1 m/s and 44 kN at 2 m/s. Consistent with theory, the impact force does not depend on the total mass of the projectile.

It is interesting to compare these results with the predicted values from Eq. (1). When Eq. (1) is nondimensionalized with Eq. (9), and Δt is taken to be t_L, Eq. (1) reduces to $\pi/2$, or approximately 1.57. However, ASCE 7 suggests Δt = 0.03 s, whereas for the 2 m projectile Δt = 0.00039 s. Of course, the recommended value of 0.03 s is meant for a longer object, but a 12.2 m (40 ft) log would have a Δt of approximately 0.0077 s. Therefore, following ASCE 7 may underpredict the actual impact force.

The model accuracy for impact duration was examined for each case. The non-dimensional durations are shown in Fig. 10. From the force time histories, such as shown in Figs. 4-7, the duration of impact was determined as follows. The start time was defined as the point where the force recording exceeded at least 1% of the maximum recorded force value. The end time was defined as the point at which the force becomes zero. In some cases, the force did not reach zero. Instead, for a very short duration of time, the force decreased to a very low value followed by a rise. In those cases, end time was defined as the time at minimal peak force in the sustained force plateau. The measured time durations were nondimensionalized by t_L. For a 1 m projectile, 2 t_L is approximately 0.387 ms. This value can be multiplied by the projectile length to obtain the factors for other lengths. The results agree reasonably well with the one-dimensional analytical model

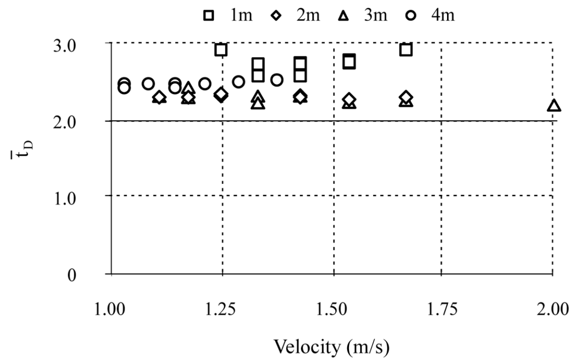

Fig. 10 Load duration versus impact velocity for different length projectiles

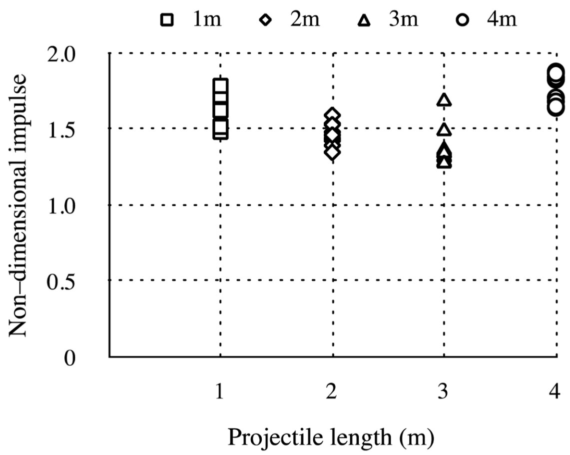

Fig. 11 Impulse calculated for nondimensionalized time and force quantities

($\bar{t}_D = 2$), although the actual durations are consistently longer. This is due likely to the gradual, initially uneven contact.

The force time histories, such as in Figs. 4-7, were integrated to obtain the total force impulse as a result of impact. These values are compared with the theoretical value of 2.0 in Fig. 11. Even though the theoretical duration underpredicts the experimental value, the theoretical value for impulse overpredicts the impulse. Hence, the theoretical model is conservative in terms of impulse.

The average strain time histories at two sections for the 2 m projectile with six strain gauges and 1.54 m/s velocity are shown in Fig. 12. The strain recordings were used to extract the propagation speeds. For each of the projectiles, two trials with 6 strain sensors were used to verify the speed of sound. For each of the strain gauge locations, the strain increase time stamp was extracted and, based on the projectile length, the propagations speeds were calculated. The extracted values resulted in approximately c_p = 5600 m/s, which is within the range of values for steel provided in the literature.

Forces can be calculated from the measured strains by multiplying by E_pA_p. The agreement of these forces with the measured forces, however, varied widely. The reasons for the wide variation are unclear, but it is quite possible that two strain gauges on a cross section are insufficient to capture the strain variation. For both the load cell forces, Fig. 5, and the strains, Fig. 12, the times

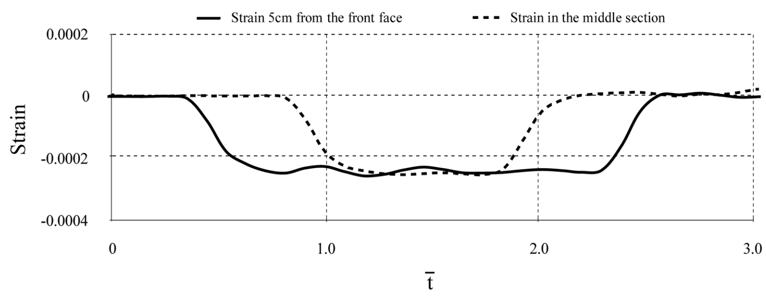

Fig. 12 Sample strain time history for one of the trials

to reach the first maximum after initial impact were similar. This implies that the gradual rise in impact force shown in the load cell is due not to the dynamics of the load cell, but to the contact between the projectile and the front plate. However, comparison of the oscillations in Fig. 5 and Fig. 12 indicate that the larger oscillations in the load cell force time history may be due to the dynamics of the load cell.

5. Finite Element (FE) model and results

A linear finite element model was developed to investigate the physics of the impact event. The model was created using ABAQUS Explicit 6.1 (Dassault Systémes). The tube, contact plate, and load cell were modeled using 8-node solid brick elements and 6 node solid wedge elements (C3D8 and C3D6 (Dassault Systemés)), as illustrated in Fig. 13.

The internal structure of the load cell was not known. Therefore, the load cell assembly was modeled as a square plate and a hollow cylinder. A cylinder thickness of 0.575 cm was chosen to

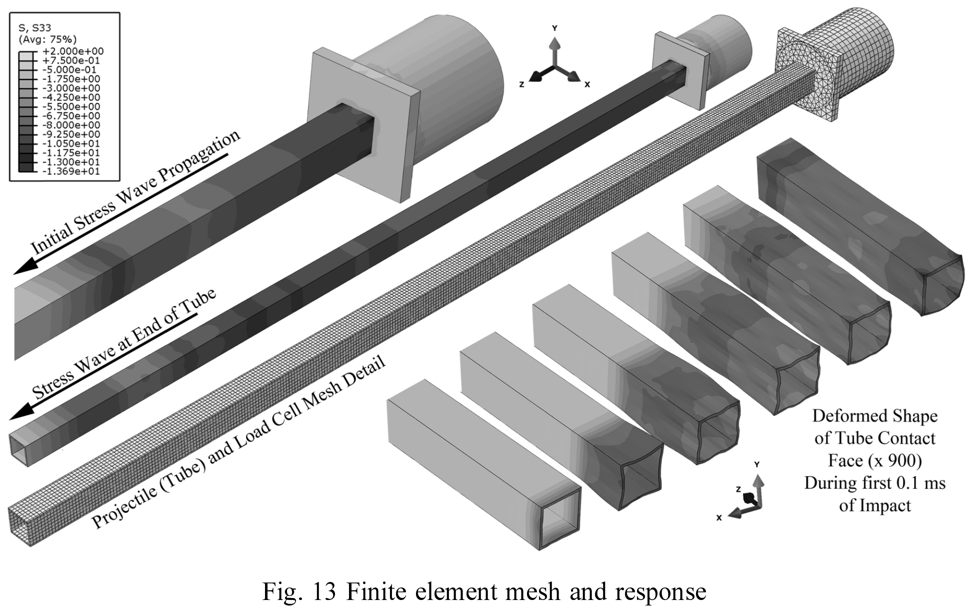

Fig. 13 Finite element mesh and response

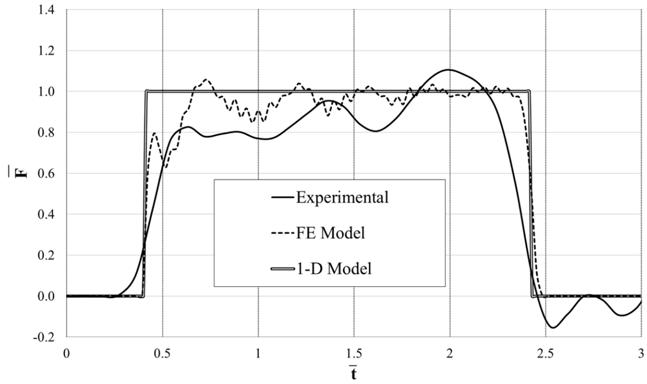

Fig. 14 Nondimensionalized force time histories

match the manufacturer specified load cell stiffness. The model cylinder section correlated with the measured length and external diameter of 17.78 cm and 15.24 cm, respectively. The density of the front plate was modified to equal the measured mass of the plate with holes. The density of the cylinder was chosen to provide an axial period of 3.9 ms, which is comparable to the measured period (3.6-4.0 ms) of the load cell and support as discussed above. The plate and cylinder densities used were 7630 kg/m^3 and 5878×10^3 kg/m^3, respectively. Poisson's ratio of 0.3 and a modulus of 200 GPa were used for all components.

5.1 FE and 1-D model results

Fig. 14 shows the time history of nondimensionalized experimental and finite element contact forces for a 2 m projectile, as well as the 1-D model force. In the figure, FE Model is the contact force calculated by ABAQUS between the interface of the projectile and the front plate on the load cell. The FE contact force correlates well with the predicted applied force from the 1-D model and the experimental load cell data. The model provides an immediate jump in the contact force, which is not seen in Figs. 4-7 or Fig. 12 for the experimental data. This abrupt increase is associated with a perfect planar impact surface, which is hard to achieve in the lab. The FE model exhibits a harmonic oscillation in the contact force. For the case examined the period of the oscillation is approximately 0.14 ms. It is possible that this high frequency variation in contact force is due to the higher mode response of the projectile (tube), which is illustrated in Fig. 13.

6. Conclusions

A simple one-dimensional analytical model has been developed to estimate the force time history imparted to structures subjected to longitudinal impact from debris. The model is based on stress propagation in a 1-D bar. Based on results from a small scale experimental program, the model gives good agreement for both the maximum impact force and the duration of impact. In addition the method provides a conservative estimate of impulse energy. It is clear that real impact does not involve immediate and full contact between the debris and the structure. The result is that the sudden impact that would otherwise occur is actually a gradual impact that builds up to the maximum impact force. As shown, addition of a 'contact stiffness' can replicate this behavior. The results indicate that the model provides an accurate estimation of the peak impact force and its duration. It also confirms that for the impact scenario considered herein, the maximum impact force does not depend on the total mass of the debris, as is often assumed in code provisions based on rigid body impact. For large and heavy debris, such as shipping containers, this may be an important point. The results are also useful to aid in the design of larger scale impact experiments, such as with full scale shipping containers, so as to quantify impact forces that might be experienced in the field.

Three-dimensional FE modeling has confirmed that the 1-D analytical model provides a reasonable method of estimating impact forces and durations, confirming that the analytical model provides a good approximation of the impact event. Both models give a conservative result when analyzed without a contact stiffness parameter.

The analytical model has been enhanced to include the acoustic waves in a water column behind the projectile. This model indicates when the fluid may increase the force and/or duration of the impact, and the parameters that control this.

Only the small time-scale acoustic response of the impact event has been considered here. Further work should also consider the longer time-scale gravity waves induced by the impact event, including the free surface. Subsequent finite element modeling should preferably include a more physically-faithful model of the load cell.

Acknowledgements

This material is based upon work supported by the National Science Foundation through the George E. Brown, Jr. Network for Earthquake Engineering Simulation under grant CMMI-1041666. This funding is gratefully acknowledged.

References

AASHTO (2009), "Vessel collision design of highway bridges", American Association of State Highway and Transportation Officials, 217.

Arroyo-Caraballo, J.R. and Ebeling, R.M. (2006), "Glancing-blow impact forces by a barge train on a lock approach wall", *J. Infrastruct. Syst.*, **5**, 135-143.

ASCE (2006), "Minimum design loads for buildings and other structures", ASCE/SEI 7-05, American Society of Civil Engineers.

Consolazio, G.R. and Cowan, D.R. (2005), "Numerically efficient dynamic analysis of barge collisions with bridge piers", *J. Struct. Eng.*, **8**, 1256-1266.

Consolazio, G.R., Cook, R.A., McVay, M.C., Cowan, D., Biggs, A. and Bui, L. (2006), "Barge impact testing of the St. George Island causeway bridge", UF 00026868/FDOT BC-354 RPWO 76, University of Florida, Gainesville, FL.

Consolazio, G.R., Getter, D.J. and Davidson, M.T. (2009), "A static analysis method for barge-impact design of bridges with consideration of dynamic amplification", UF Project No. 00068901/FDOT BD-545-85, University of Florida, Gainsville, FL.

Dassault Systèmes, Abaqus Unified FEA Software, Ver. 6.10, Dassault Systèmes Simulia Corp., Providence, RI, USA.

FEMA (2005), Coastal Construction Manual, FEMA P-55, Edition 3, Vol. 2, Federal Emergency Management Agency, Washington, D.C.

FEMA (2008), "Guidelines for design of structures for vertical evacuation from tsunamis", FEMA P646, Federal Emergency Management Agency.

Goldsmith, W. (1960), *Impact: The Theory and Physical Behaviour of Colliding Solids*, Edward Arnold Ltd., London.

Haehnel, R.B. and Daly, S.F. (2002), "Maximum impact force of woody debris on floodplain structures", ERDC/CRREL TR-02-2, US Army Corp of Engineers, Engineer Research and Development Center.

Haehnel, R.B. and Daly, S.F. (2004), "Maximum impact force of woody debris on floodplain structures", *J. Hydraulic Eng.*, **2**, 112-120.

Johnson, W. (1972), *Impact Strength of Materials*, Edward Arnold, London, .

Kumagai, K., Oda, K. and Fujii, N. (2006), "Applicability of simulation model for drift behavior of containers due to tsunami", *Techno-Ocean 2006/19th JASNAOE Ocean Engineering Symposium*, Kobe, Japan.

Matsutomi, H. (2009), "Method for estimating collision force of driftwood accompanying tsunami inundation flow", *J. Disaster Res.*, **6**, 435-440.

Mikhaylov, Y. (2009), "Evaluation of prototypical reinforced concrete building performance when subjected to tsunami loading", M.S. Thesis, University of Hawaii, USA.

Mizutani, N., Takagi, Y., Shiraishi, K., Miyajima, S. and Tomita, T. (2005), "Study on wave force on a container on apron due to tsunamis and collision force of drifted container", *Annual Journal of Coastal Engineering*, 741-745.

NRC (2004), *Preventing Earthquake Disasters: The Grand Challenge in Earthquake Engineering: A Research Agenda for the Network for Earthquake Engineering Simulation (NEES)*, The National Academies Press, Washington, D.C..

Oda, K., Okamoto, O. and Kumagai, K. (2006), "Development of estimation method on drift and collision behaviors of debris caused by tsunamis", *Tech. Memorandum of Public Works Research Institute*.

Robertson, I.N., Riggs, H.R., Yim, S.C.S. and Young, Y.L. (2006), "Lessons from Katrina", *Civil Engineering, ASCE Magazine*, April, 56-63.

USACE (2004), *Barge Impact Analysis for Rigid Walls*, ETL 1110-2-563, USACE, Washington, DC.

Yeh, H. (2007), "Design tsunami forces for onshore structures", *J. Disaster Res.*, **6**, 1-6.

Yeom, G.S., Nakamura, T. and Mizutani, N. (2009), "Collision analysis of container drifted by runup tsunami using drift collision coupled model", *J. Disaster Res.*, **6**, 441-449.